Supporting Information

Dumbbell-like $Au_{0.5}Cu_{0.5}@Fe_3O_4$ Nanocrystals: Synthesis, Characterization and Catalytic Activity in CO Oxidation

Sharif Najafishirtari,[a,c] Tathiana Midori Kokumai,[b] Sergio Marras,[a] Priscila Destro,[b] Mirko Prato,[a] Alice Scarpellini,[a] Rosaria Brescia,[a] Aidin Lak,[d] Teresa Pellegrino,[d] Daniela Zanchet,[b] Liberato Manna,[a] Massimo Colombo[a]*

a) Department of Nanochemistry, Istituto Italiano di Tecnologia, Via Morego 30, 16163, Genova, Italy.

b) Institute of Chemistry, University of Campinas (UNICAMP), P.O. Box 6154, 13083-970 Campinas, São Paulo, Brazil.

c) Dipartimento di Chimica e Chimica Industriale, Università di Genova, via Dodecaneso 31- I-16146 Genova, Italy.

d) Drug Discovery and Development, Istituto Italiano di Tecnologia, Via Morego 30, 16163 Genova, Italy.

massimo.colombo@iit.it (corresponding author email)

Movie IS1: Aligned tilt series of HAADF-STEM images on the AuCu@FeOx heterostructures, collected from -70° to +50°. in steps of 2° at high angles and 5° from -30° to +30°. The full frame size is 327.68 nm and the rotation axis is vertical and centered in the image.

Removal of Chlorine species from catalyst surface

The presence of Cl on the dumbbell catalyst even after the calcination step was verified by two different methods. We firstly washed the catalyst sample with warm water (~ 40 °C), collected the supernatant solution and mixed it with a $AgNO_3$ solution: precipitation of AgCl was clearly observed in case of AuCu@FeOx/Alumina (see Figure S1) and Au@FeOx/Alumina (not shown), while no precipitate was formed in case of AuCu/Magnetite sample. We also obtained indirect evidence of the presence of residual Cl in the non-washed catalysts by collecting the catalytic activity data in CO oxidation. As shown in Figure S2, the non-washed AuCu@FeOx/Alumina catalyst showed much lower activity than the washed sample, in line with the well-known poisoning effect of Cl on the CO oxidation activity of Au based catalysts [1-2]. The same trend was observed over the Au@FeOx/Alumina sample (not shown). In case of AuCu/Magnetite catalyst, no significant difference in the catalytic activity was observed between the washed and non-washed samples. Compared to the AuCu/Magnetite sample, the only additional source of Cl in case of the dumbbells samples was the solvent in which the dumbbell NCs were dispersed (i.e. chloroform). Based on these results, it seems plausible that the calcination step in the static air caused the decomposition/combustion of residual chloroform and consequently Cl poisoning of the AuCu@FeOx/Alumina and Au@FeOx/Alumina samples. Another possibility is that the Cl had a different affinity for the different supports (i.e. alumina vs. magnetite), leading thus to a different effect of the washing procedure. Though the detailed understanding of this phenomenon is not in the scope of the present work, washing of the dumbbell catalyst was nevertheless essential to attain the highest level of activity in CO oxidation.

Figure S1. Successful removal of the Cl from the calcined dumbbell catalyst. The left vial contains plain deionized water used for the washing step; the middle vial contains the supernatant recovered after the first washing step of the AuCu@FeOx/Alumina dumbbell catalyst and addition of 400 µl of $AgNO_3$ (0.5 M). The right vial contains the supernatant recovered after washing of the bare Alumina support and addition of the same $AgNO_3$ solution.

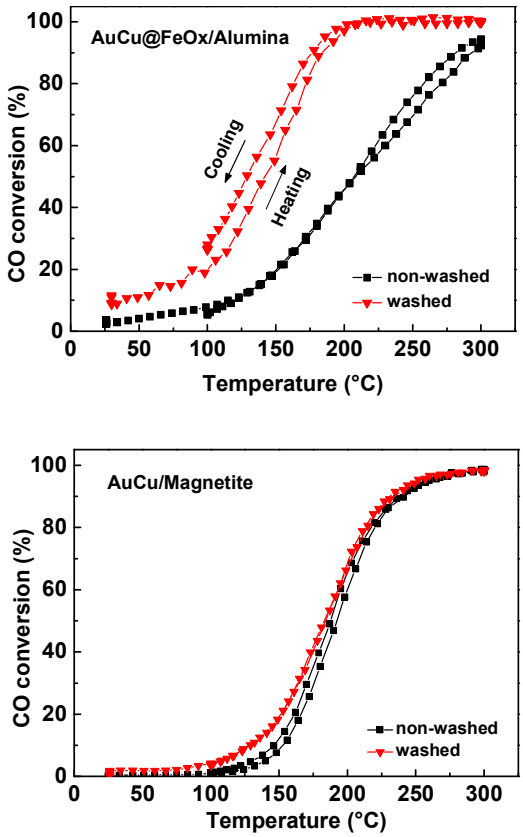

Figure S2. Comparison of the CO oxidation activity for the washed and non-washed AuCu@FeOx/Al_2O_3 and AuCu/Magnetite catalysts. Experimental conditions: CO = 1% v/v; O_2 = 6% v/v; WHSV= 3'000'000 Ncc/h/g(Au+Cu).

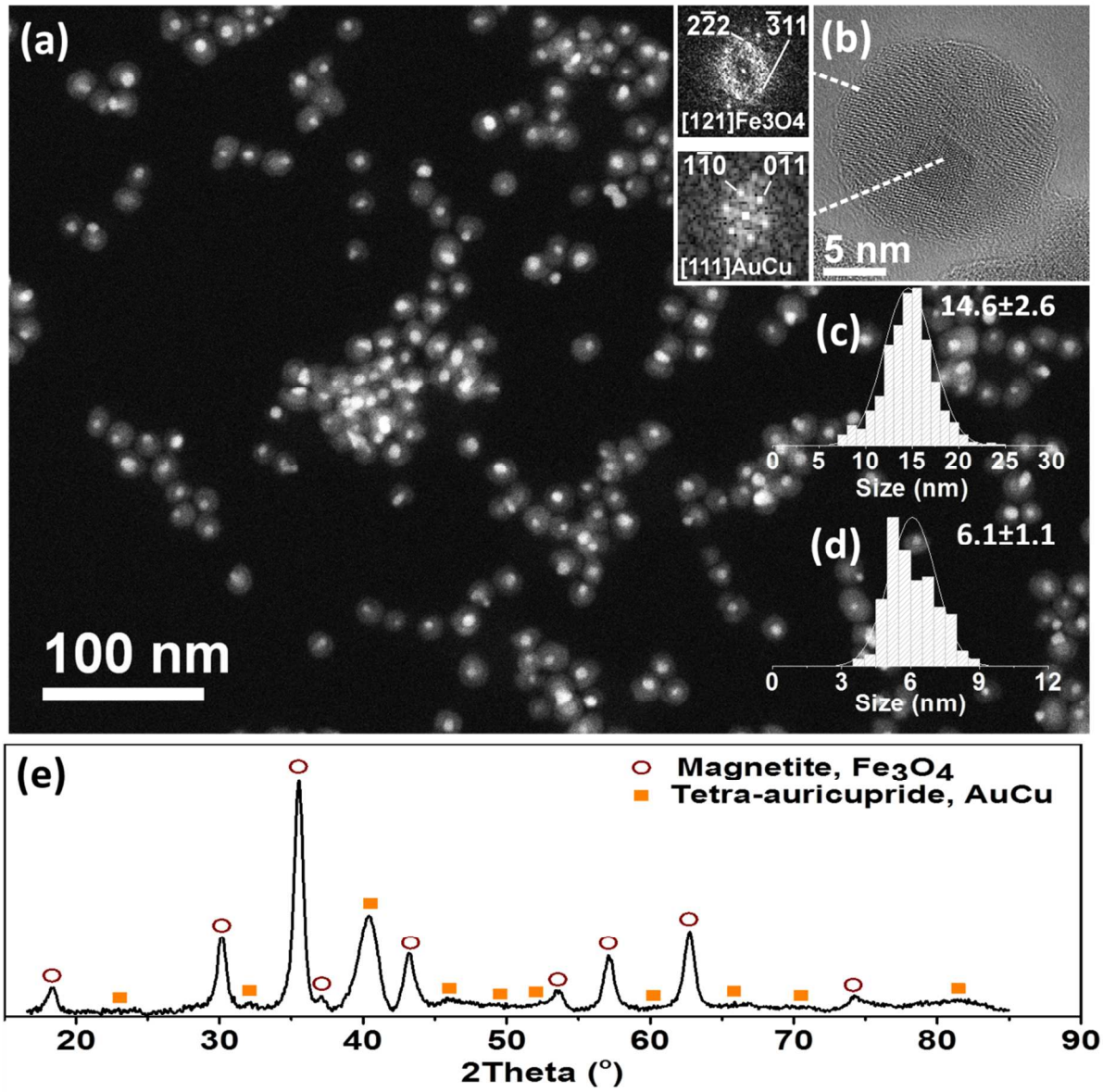

Figure S3. (a) Typical HAADF-STEM image of the as-prepared AuCu@FeOx colloidal NCs. (b) HRTEM image of a single NC. (c) Size distribution histograms of FeOx and (d) AuCu domains obtained by graphical analysis. (e) X-ray diffraction (XRD) pattern of the as-synthesized AuCu@FeOx dumbbell NCs. Experimental data are compared with the database powder XRD patterns for tetragonal AuCu (ICSD code: 42574) and magnetite Fe_3O_4 (ICSD code: 65341).

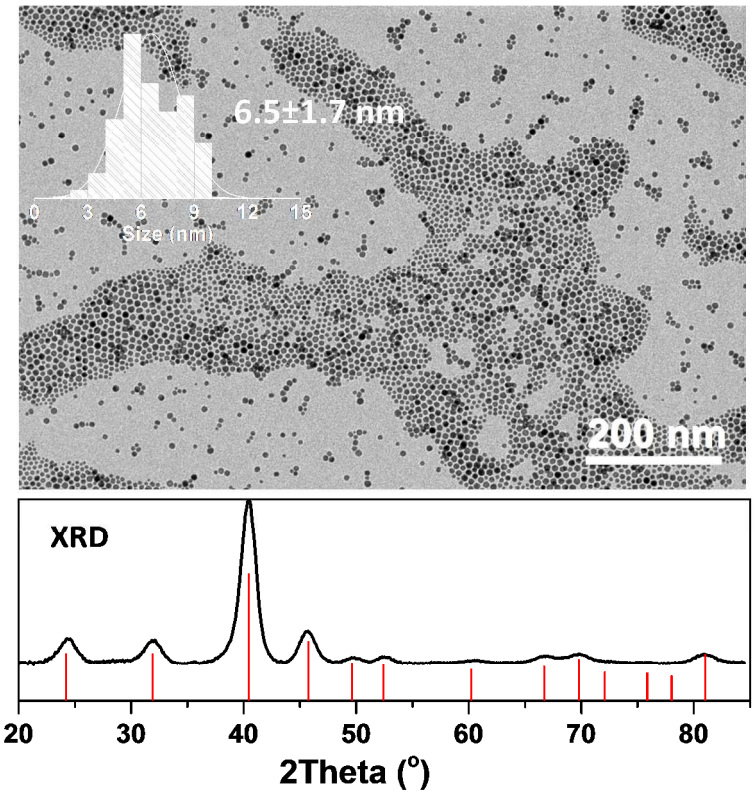

Figure S4. Typical bright-field (BF)-TEM image of the as-prepared AuCu colloidal NCs; top left inset: size distribution obtained by measuring ~3500 NCs; the XRD pattern of AuCu seeds at the bottom. Experimental data are compared with the database powder XRD pattern for tetragonal AuCu (ICSD code: 42574);

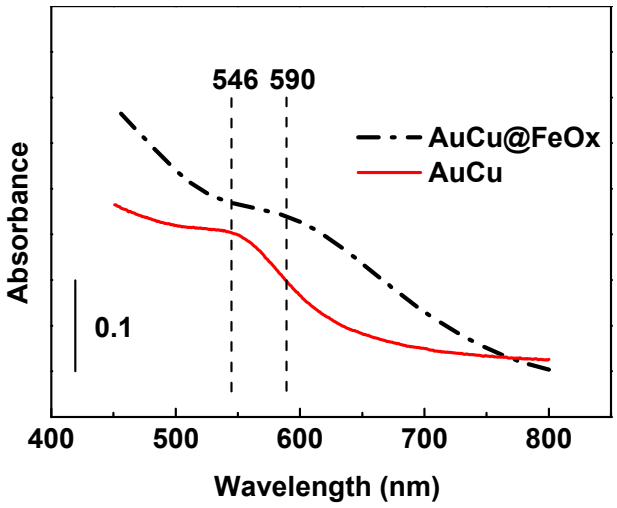

Figure S5. Absorption spectra for AuCu (thin red line) and AuCu@FeOx (thick black dash-dot line) NCs dispersed in hexane and chloroform, respectively. The background spectrum of the solvent was collected before each measurement.

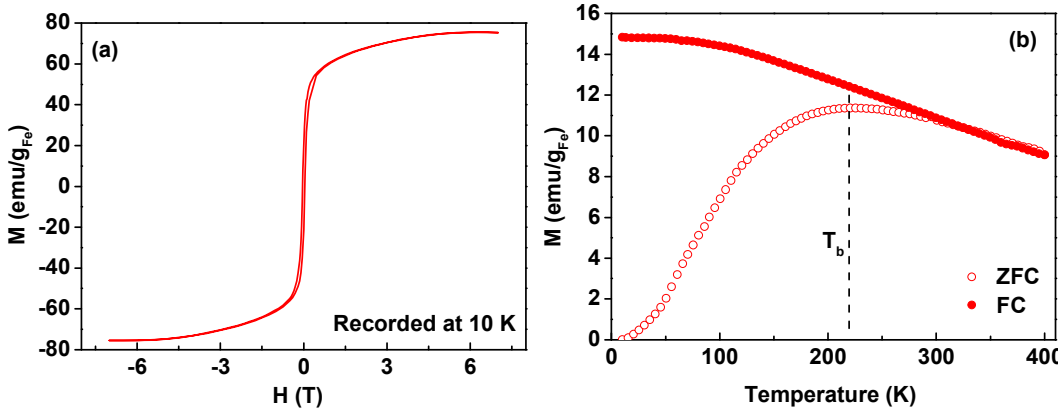

Figure S6. (a) Magnetization versus field (*M-H*) measured at 10 K and (b) zero-field-cooled (ZFC) and field-cooled (FC) temperature dependent magnetization curves recorded on the dumbbell NCs in the cooling field of 5 mT .

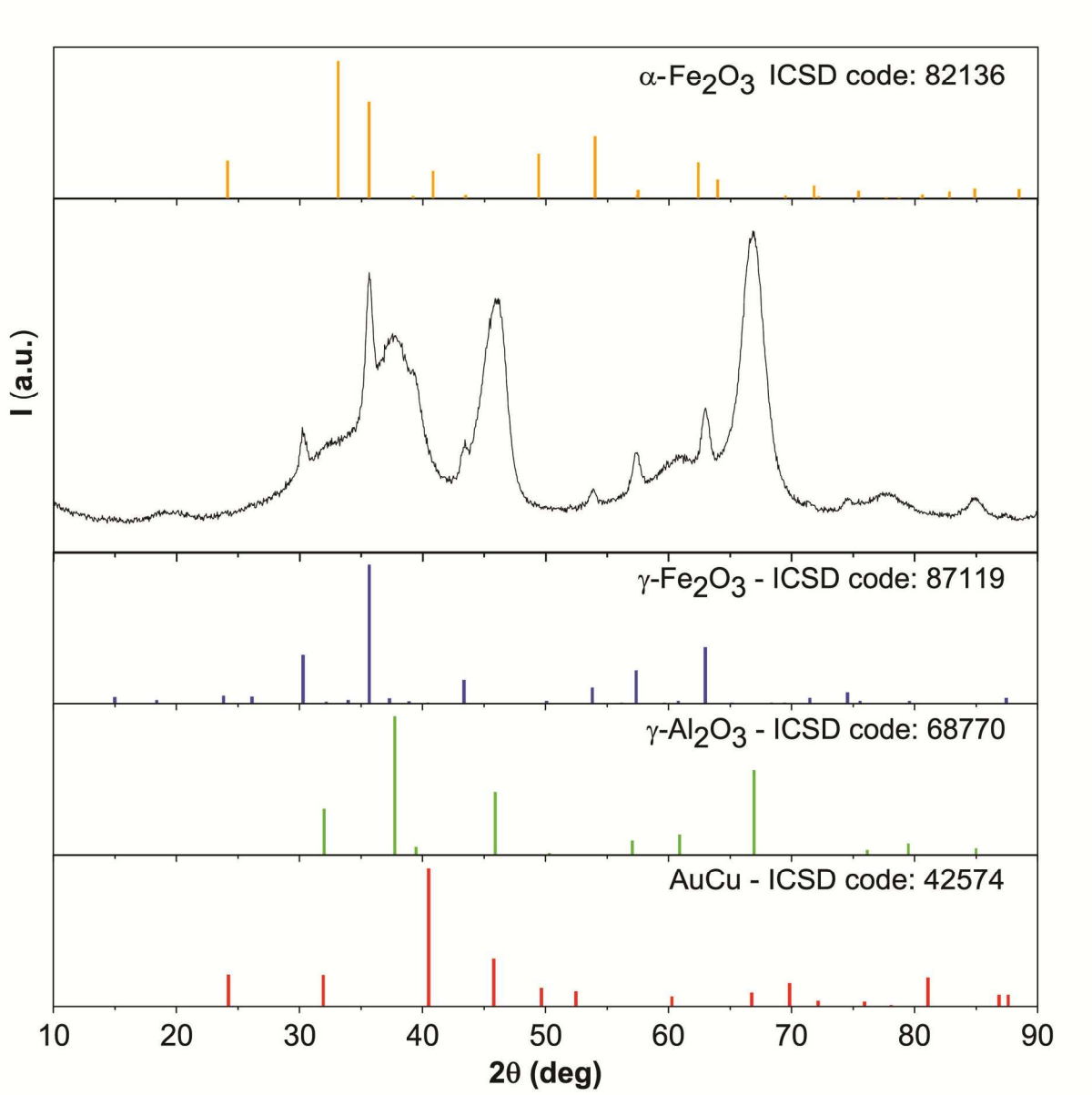

Figure S7. X-ray diffraction (XRD) patterns of AuCu@FeOx/Alumina catalyst after activation. Experimental data are compared with the database powder XRD patterns for maghemite (ICSD code: 87119), hematite (ICSD code: 82136), γ-Al_2O_3 (ICSD code: 68770) and AuCu (ICSD code: 42574).

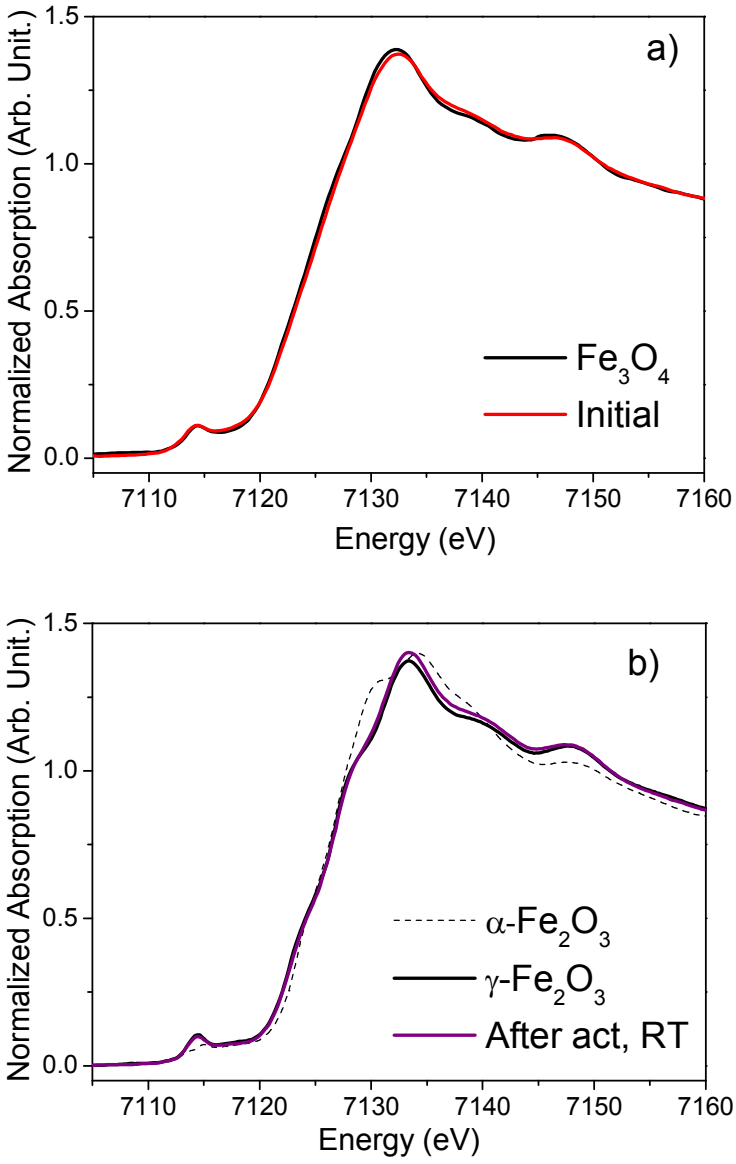

Figure S8. Comparison of the Fe K-edge XANES spectra of a) the fresh AuCu@FeOx/Alumina catalyst against bulk magnetite and b) the activated AuCu@FeOx/Alumina catalyst against bulk maghemite (γ-Fe_2O_3) and hematite (α-Fe_2O_3)..

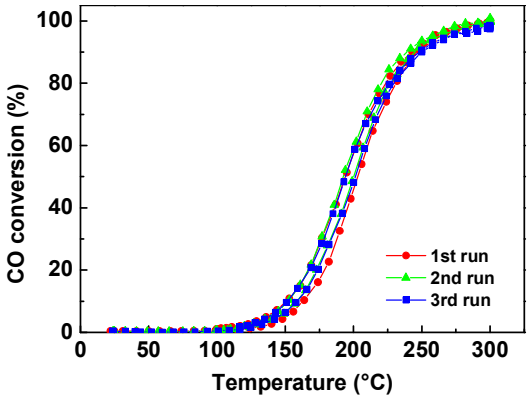

Figure S9. Stability of the AuCu/Magnetite catalysts proved by reproducibility of the catalytic activity data in CO oxidation in three consecutive cycles of transient test after oxidative pre-treatment; Experimental conditions: CO = 1% v/v; O_2 = 6% v/v; WHSV= 3'000'000 Ncc/h/g(Au+Cu).

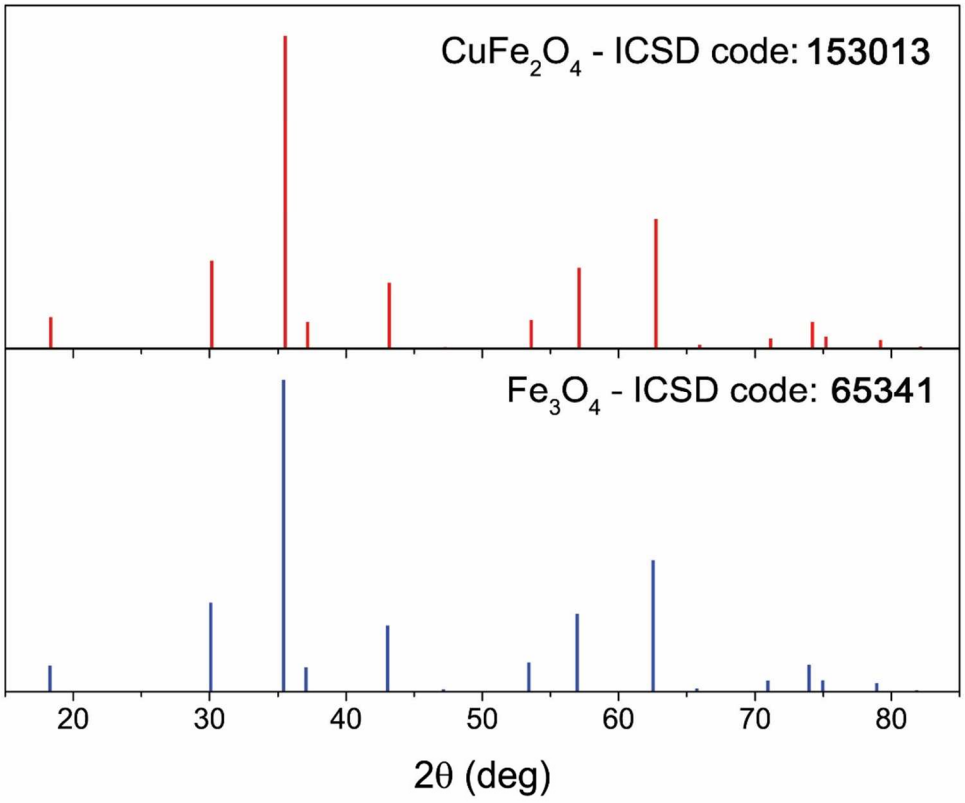

Figure S10. XRD reference patterns for magnetite (ICSD code 65341) and cuprospinel (ICSD code 153013).

Table S1. Semi-quantitative analysis based on Reference Intensity Ratio (RIR).

Sample	Cuprospinel (ICSD code 153013)	Gold (ICSD code 44362)	Hematite (ICSD code 82136)	Cu moles from RIR	Cu moles from ICP
Activated AuCu/Magnetite	6.8 ± 0.1 wt. %	1.1 ± 0.01wt.%	92.1 ± 0.01 wt. %	0.0284	0.0041
AuCu/Magnetite further annealed for 10h at 350°C in air	0.8 ± 0.3 wt. %	0.9 ± 0.04 wt.%	98.3 ± 0.01 wt. %	0.0033	0.0041

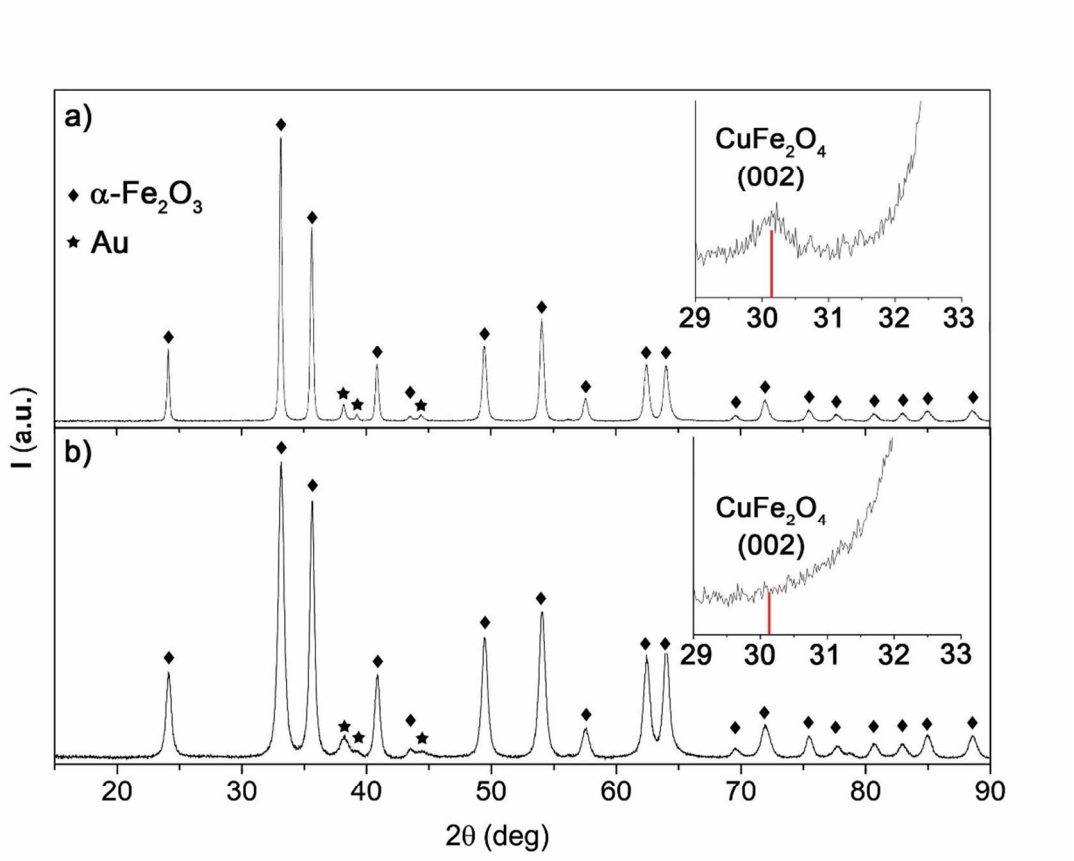

Figure S11. X-ray diffraction (XRD) patterns of (a) AuCu/Magnetite and (b) Au/Magnetite after further calcination in air for 10 h at 350 ºC. Experimental data are compared with the database powder XRD patterns for hematite (ICSD code: 82136), cuprospinel (ICSD code: 153013) and Au (ICSD code:

44362). The data presented in the insets were obtained using a reduced scan speed of 0.01 °/min. The reduced scan speed was necessary in order to increase the signal to noise ratio and resolve the weak pattern of the cuprospinel phase.

Evaluation of Turn over Frequency (TOF):

We report the rate of reaction as:

$$\frac{molCO2\text{produced}}{s} = \frac{COfeed\,(Ncc/\min)\cdot COconversion}{60\,(s/\min)\cdot 22.414\,(cc/mol)}$$

We assumed spherical Au domains and considered that only half of the sphere was exposed to the reacting atmosphere (i.e. half of the sphere is embedded in the iron oxide domain). The content of gold was measured by ICP. We consider bulk gold density and the area occupied by surface gold atoms to be 1.9 E-5 mol/m^2 [3]. TOF was thus calculated as:

$$TOF = \frac{molCO\,2\text{produced}}{s}\cdot\frac{1}{molAu}$$

References

(1) Oh, H. S.; Yang, J. H.; Costello, C. K.; Wang, Y. M.; Bare, S. R.; Kung, H. H.; Kung, M. C. Selective Catalytic Oxidation of CO: Effect of Chloride on Supported Au Catalysts, *J Catal.* **2002**, *210* (2), 375-386.

(2) Broqvist, P.; Molina, L. M.; Grönbeck, H.; Hammer, B. Promoting and Poisoning Effects of Na and Cl Coadsorption on CO Oxidation over MgO-Supported Au Nanoparticles, *J. Catal*. **2004**, *227* (1), 217-226.

(3) Güttel, R.; Paul, M.; Galeano, C.; Schüth, F. Au, @ZrO_2 Yolk–Shell Catalysts for CO Oxidation: Study of Particle Size Effect by Ex-post Size Control of Au Cores, *J. Catal*. **2012**, *289*, 100-104